



# Linker functionalized poly(heptazine imide) as charge channel and activation site for enhancing photocatalytic nitrogen fixation in pure water

Shilian Yang<sup>a,1</sup>, Xiaoxu Deng<sup>b,1</sup>, Peng Chen<sup>a,\*</sup>, Tianxiang Zhao<sup>a</sup>, Fei liu<sup>a</sup>, Chaoyong Deng<sup>b,\*</sup>, Shuang-Feng Yin<sup>c,\*</sup>

<sup>a</sup> Provincial Guizhou Key Laboratory of Green Chemical and Clean Energy Technology, School of Chemistry and Chemical Engineering, Guizhou University, Guiyang 550025, Guizhou, China

<sup>b</sup> College of Big Data and Information Engineering, Guizhou University, Guiyang 550025, Guizhou, China

<sup>c</sup> State Key Laboratory of Chemo/Biosensing and Chemometrics, Advanced Catalytic Engineering Research Center of the Ministry of Education, College of Chemistry and Chemical Engineering, Hunan University, Changsha 410082, Hunan, China

## ARTICLE INFO

### Keywords:

Poly(heptazine imide)  
Photocatalysis  
Linker  
Nitrogen fixation  
Copolymerizing

## ABSTRACT

Poly(heptazine imide) as a metal-free semiconductor has stimulated considerable focus in the photocatalytic nitrogen fixation. However, the weak visible light absorption and unordered migration of photogenerated carriers as well as limited active site often resulted in poor photocatalytic performance. Here, we propose a conceptual to construct directional electron delivery channel via introducing C-N and N-C-O units linked terminal melem units (PCON) using a facile copolymerizing method. The optimized PCON achieved excellent photocatalytic nitrogen fixation rate ( $49.11 \mu\text{mol g}^{-1} \text{h}^{-1}$ ) and near-IR yield in pure water without using cocatalyst, which is 11 times higher than that of pristine  $\text{C}_3\text{N}_4$ . Based on DFT calculation and experiment results, the superior photocatalytic performance is traced back to the integrated different linker into the framework induced  $n - \pi^*$  transitions and acted as charge channel and activation site, which could significantly extend light absorption to the near IR, and enhance charge separation as well as reactive activation. This study lay out the importance of linker engineer of the catalyst to regulate photocatalytic activity over organic-based photocatalysts.

## 1. Introduction

Ammonia synthesis from the reduction of  $\text{N}_2$  atmosphere is an essential and challenging chemical transformation to modern industry and agriculture [1–3]. Currently, the industrial Haber-Bosch process often suffers from harsh reaction conditions and considerable energy consumption, rendering a huge amount of environmental and energy issues [4]. Photocatalytic  $\text{N}_2$  reduction reaction (NRR) has been regarded as a promising, sustainable and cost-effective strategy to produce  $\text{NH}_3$  directly under mild conditions. Despite its greater prospects, the system is often hindered by the high  $\text{N}\equiv\text{N}$  bond dissociation energy ( $941 \text{ kJ mol}^{-1}$ ) and simultaneous the low kinetics of  $\text{H}_2\text{O}$  oxidation, resulting in poor quantum yield [5,6]. Moreover, a large number of NRR reactions were implemented in sacrificial agent system, which greatly impeded the practical application of photocatalysis [7,8]. To overcome these limits, it is highly urgent to seek efficient and novel systems for

## NRR.

To date, a great deal of photocatalysts such as  $\text{TiO}_2$ ,  $\text{Bi}_2\text{WO}_6$ ,  $\text{Fe}_2\text{O}_3$ ,  $\text{CuO}$  and  $\text{BiOBr}$  et al. have been investigated for NRR [9,10]. Considering the tunable electronic property, suitable band gap, long durability and low price, carbon nitride has attracted widespread attention in photocatalytic ammonia production [11,12]. Among the known carbon nitrides, poly(heptazine imide) exhibits highly efficient photocatalytic activity due to its light absorption and photogenerated electron storage properties through the use of N-H groups [13,14]. However, similar to other conventional photocatalysts, poly(heptazine imide) also suffered from weak light response range, rapid recombination of carriers, and lack of effective active sites, which handicaps the high performance of photocatalysis [15]. Various approaches, containing doping, forming heterostructure, and functionalization have been developed to amend drawbacks of poly(heptazine imide) [16,17]. Zhang et al. confirmed that the melem unit made predominated role in light absorption to produce

\* Corresponding authors.

E-mail addresses: [pchen3@gzu.edu.cn](mailto:pchen3@gzu.edu.cn) (P. Chen), [cydeng@gzu.edu.cn](mailto:cydeng@gzu.edu.cn) (C. Deng), [sf\\_yin@hnu.edu.cn](mailto:sf_yin@hnu.edu.cn) (S.-F. Yin).

<sup>1</sup> S. Yang and X. Deng contribute equally to this work.

electron hole pair [18]. Therefore, the direct atomic modifying of melem units is not the best option. Rational modulating functional groups in the edge sites or chain structure is the intrinsic force to control the electron mobility, energy band structure and surface reaction. Lotsch et al. have rational designed large amounts of edge sites to functionalize heptazine-based polymer for enhancing the separation of the photo-generated charge carriers [19]. Nevertheless, the light absorption properties are not significant improvement using edge sites modification strategies. Kumar et al. reported heptazine moiety linked with azo nitrogens in the carbon nitride skeleton has extended the optical absorption to the near infrared region [20]. However, due to the highly symmetric structure, the improvement of photocatalytic performance is still limited. Zheng et al. reported that the localized asymmetry of the structure not only form the separate positive and negative charge centers, but also adjust the surface properties and energy band structure of the material [21]. To the best of our knowledge, rare work has focused on the modification of different functional linkage on the heptazine imide monomer-based polymer. Therefore, an effective strategy to embellish different groups on the linkage of poly(heptazine imide) is urgently needed.

Inspired by the aforementioned points, different linker species (containing C-N and N-C-O units) embed in the poly(heptazine imide) have been prepared via a monomer-directed copolymerization strategy. Impressively, PCON represented remarkable activity in photocatalytic  $N_2$  fixation in the pure water under visible light irradiation, receiving a brilliant  $NH_3$  production rate ( $49.11 \mu\text{mol g}^{-1} \text{h}^{-1}$ ) without any cocatalyst at room temperature, which was 11 times higher than  $g\text{-C}_3\text{N}_4$  and the other reported metal-free catalyst. More importantly, the PCON still maintained considerable  $NH_3$  production under the near-IR (750 nm) monochromatic light illumination. DFT calculation and experiment results shows that the different linker significantly enhanced the light absorption, carrier mobility and surface properties of poly(heptazine imide). Taken together, this strategy highlights the importance of linkage engineering in the development of high-performance polymer for nitrogen fixation.

## 2. Experimental section

### 2.1. Synthesis of PCON

The different linker species (containing C-N and N-C-O units) embed in the poly(heptazine imide) (PCON) have been prepared via a monomer-directed copolymerization strategy. Firstly, melem hydrazine was synthesized by following Kumar et al reported literature. 4.414 g of melem hydrazine and 1.673 g of formaldehyde aqueous solutions were added to 100 mL of vigorously stirred water. The pH of the mixture solution was adjusted to 8.4 by adding appropriate amount of triethanolamine. Then, the alkaline solution was stirred in a water bath with  $80^\circ\text{C}$  for 2 h. Subsequently, a certain concentration of hydrochloric acid was added the above solution hydrochloric acid ( $\text{pH} = 2$ ). After stirring for 1.5 h, the precursor was collected by filtration and drying. Finally, PCON-2 was synthesized by the calcination of precursor at  $500^\circ\text{C}$  in a tube furnace under nitrogen for 2 h. For comparison, PCON-1 and PCON-3 were obtained by calcination at  $450^\circ\text{C}$  and  $550^\circ\text{C}$ , respectively.

### 2.2. Synthesis of $C_3N_4$ and $C_3N_5$

Typically, the 5 g of melamine was put into a crucible and then heated to  $500^\circ\text{C}$  for 2 h under nitrogen atmosphere.  $C_3N_5$  was prepared by heating melem hydrazine in the same condition [19].

### 2.3. Catalyst characterizations

The structure of catalyst were analyzed by X-ray diffraction (XRD, Bruker D8 Advance). X-ray photoelectron spectroscopy (XPS) measurements were carried out with Thermo Fisher K-Alpha Plus. PCON

powder was measured on a Fourier Transform Infrared spectrometer (FT-IR, Shimadzu IR Affinity-1). Brunauer–Emmett–Teller (BET) surface areas were explored with a nitrogen adsorption apparatus (BET, the Micrometrics ASAP 2020 and AutoChem II 2920). UV–vis spectra of the samples were obtained by an UV–vis spectrophotometer (UV–vis, Shimadzu UV-3600 plus). Scanning electron microscope (SEM, Hitachi S-4800) and transmission electron microscopy (TEM, JEM-2100 F) were used to investigate the morphology of the photocatalysts. Electrochemical impedance spectra (EIS) and photocurrents were conducted with a Chenhu electrochemical workstation (CHI660E).

### 2.4. Photocatalytic $N_2$ fixation

The photocatalytic  $N_2$  fixation of PCON was evaluated in a Pyrex reactor. Typically, 20 mg of catalyst was immersed in 100 mL of DI water with a magnetic stirring. Before the light illumination, a flow  $N_2$  ( $30 \text{ mL min}^{-1}$ ) was continuously pumped into the Pyrex reactor and stirred for half an hour. Subsequently, the mixed solution was illuminated under vigorous stirring by a Xenon lamp ( $\lambda \geq 420 \text{ nm}$ ). The production of  $NH_3$  was detected by Nessler's reagent. The apparent efficiency (AQE) was measured by using different monochromatic lights centered at 420, 450, 500, 550, 600, 700 and 750 nm. The calculated formula of AQE was followed the reported literature [22].

### 2.5. $^{15}N_2$ and $^{14}N_2$ isotope labelling experiments

Typically, with using the  $^{15}N_2$  or  $^{14}N_2$  gas in the photocatalytic  $N_2$  fixation reaction, the pH value of solution was modulated to 2 by using  $1 \text{ mol L}^{-1} \text{H}_2\text{SO}_4$ . Then,  $D_2O$  was added and mixed sufficiently. All kind of nitrogen-containing solution was test by  $^1\text{H}$  nuclear magnetic resonance (NMR, Bruker).

### 2.6. In situ FTIR test

The in-situ FT-IR measurement was tested by Shimadzu IR Affinity-1 spectrometer equipped with a custom chamber. Routinely, a certain amount of liquid nitrogen is filled into the chamber, and the PCON-2 is wetted with water. Under light illumination, the in-situ infrared spectrum was recorded by the infrared software for interval ten minutes.

### 2.7. Density Functional Theory (DFT)

The frontier electron densities of HOMO and LUMO were implemented using DMol3 package with Perdew–Burke–Ernzerhof / Double-Numerical Basis 4.4 set. The differential charge density of PCON were carried out utilizing Castep package. The cutoff energy and smearing width was 450 and 0.2 eV. A  $1 \times 1 \times 1$  K points has been chosen, and the atoms were converged to  $0.01 \text{ eV \AA}^{-1}$ .

## 3. Results and discussion

### 3.1. Preparation and characterization

The different linker containing C-N and N-C-O units in the poly(heptazine imide) skeleton have been prepared by a monomer-directed copolymerization strategy (Fig. 1). Firstly, melem hydrazine (MH) was afforded by the treatment of melem with hydrazine hydrate unites, resulting  $NH_2$  unites transformed into  $NH-NH_2$  units (Fig. S1, detailed explanation could be obtained in supporting information, SI) [19]. SEM images (Fig. S2, SI) show that melem hydrazine is rod like morphology with 100 nm of diameter. On the other hand, the  $CH_2OH$  group could insert the terminal  $NH-NH_2$  moieties of melem hydrazine to form trimethylol melem hydrazine (TMH) via MH and formaldehyde condensation reaction under alkaline conditions (Fig. S3, SI) [23,24]. A further polymerization of the TMH could be conducted under acidic conditions to generate C-N and N-C-O units in the poly(heptazine imide) [23]. Due

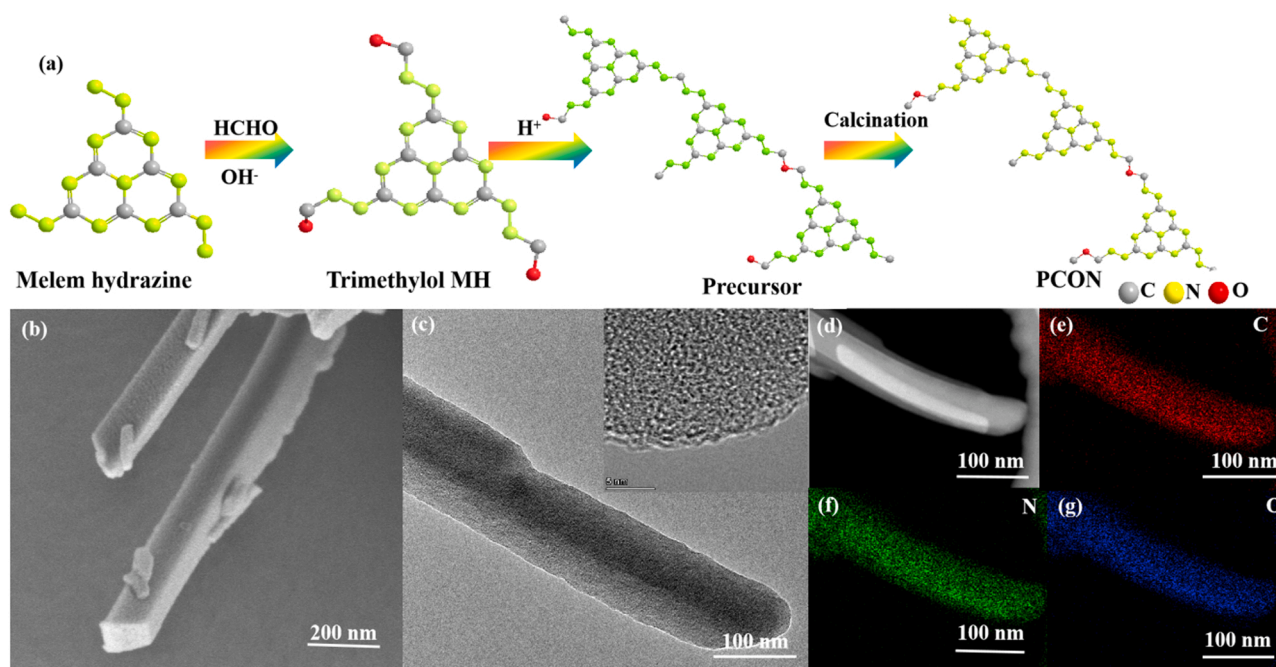


Fig. 1. (a) Schematic for the the synthesis of PCON, (b) SEM, (c) TEM and (d-f) elemental mapping images of PCON-2.

to the insufficient polymerization, the precursor possessed a large number of hydroxyl groups in the terminal group (Fig. S1 and S3, SI). Finally, several reaction conditions containing different temperature calcination was implemented to adjust the amount of C-N and N-C-O units (Table S1-S3, SI), while still further polymerization of precursor on the formed carbon nitride structure. SEM and TEM images in Fig. 1a and b reveal that the PCON is rod like morphology with about 100 nm. The corresponding elemental mapping images demonstrate that the C, N and O elements are distributed uniformly, indicating homogeneous distribution of C-N and N-C-O units in the carbon nitride framework.

The chemical structure of PCON samples were tested by X-ray diffraction (XRD) patterns,  $^{13}\text{C}$ - $^1\text{H}$  NMR and Fourier transform infrared (FTIR) spectroscopy. As depicted in Fig. 2a, there are two characteristic diffraction peaks at around  $13.61^\circ$  and  $27.08^\circ$ , which belong to the in-plane repeating of (100) and  $\pi$ - $\pi$  reflection of the (002), respectively [25]. Noteworthy, the peak of PCON at  $13.61^\circ$  became weaker in comparison with  $\text{g-C}_3\text{N}_4$ , which could be ascribed to the reduced in-plane order by inserting different groups into  $\text{g-C}_3\text{N}_4$  framework [26]. The intense diffraction peak at (002) plane for PCON shifted toward lower angles, indicating a minor increase in interlayer spacing [27]. In addition, the peak intensity of (002) in the  $\text{C}_3\text{N}_5$  and PCON displayed a palpable weak tendency compared with  $\text{C}_3\text{N}_4$ , which are ascribed to the poorer in planar periodicity via introducing the different linker in the heptazine imide unites [28]. Therefore, the disordered in-plane and interlayer structure are conducive to the separation of electrons and holes in some extent [29]. In order to further analyze the structure of the catalysts, FTIR analysis was carried out. As shown in Fig. 2b and Fig. S3, the peak centered at 1542, 1315 and  $887\text{ cm}^{-1}$  corresponded to the vibration of heptazine units [30]. Several bands at 1095, 1233, 1509 and  $3109\text{ cm}^{-1}$  are stemmed from stretching vibration of NH-NH, NH-C-NH, C-O-C and NH group [19,31].

The elemental states of the catalyst were analyzed by X-ray photoelectron spectroscopy (XPS). As shown in Fig. 2c, the PCON possess five peaks at 284.6 eV, 285.9, 287.9 and 289.3 eV, which is related to C-C/C-H, C-NH, N-C=N, and C-O bonds [32,33]. Apparently, the peak of C-NH and N-C=N bonds for the PCON sample appears slightly shift by comparing with  $\text{C}_3\text{N}_4$ , suggesting the introduction of the long chain group has adjusted the chemical environment of heptazine framework. Furthermore, the intensity ratio of C-C/N-C=N of PCON was higher

than that of  $\text{C}_3\text{N}_4$ , which could be contributed to the C-H species from the inserted carbon chains. As depicted in Table S1, the PCON-3 and PCON-1 occupied the maximum ratio of C-C/N-C=N and C-O/N-C=N, demonstrating a slightly higher content of NH-C-NH, and C-O-C bonds in the embedded framework. As shown in Fig. 2d, the N 1s of PCON-2 can be deconvoluted into four peaks at 398.3, 399.4, 400.5 and 401.5 eV, belonging to C=N-C, N-(C<sub>3</sub>), N-H and N-N bonds, respectively [19,34]. As shown in Fig. 2e, there are two peaks at 531.8 and 533.4 eV, which are related to surface adsorbed  $\text{H}_2\text{O}$  or oxygen and carbon oxygen bonds, respectively [35]. Solid state  $^{13}\text{C}$ NMR was also used to confirm the structure of the PCON. As shown in Fig. 2f, The  $^{13}\text{C}$ NMR spectrum of PCON clearly depicts two distinct peaks at 145.4 and 152.9 ppm, assigning to the N=C-N and C-NHx units in heptazine group [36]. Two small peaks emerged on the  $^{13}\text{C}$  NMR spectra at 55.2 and 47.1 ppm, which is attributed to the N-alkyl and O-alkyl groups [37]. Additionally, the  $^1\text{H}$ NMR spectra exhibits a broad protons peak around 8–10 ppm, suggesting the insertion of NH in imide bridge of heptazine backbone (Fig. S5, SI) [38]. According to the above characterization, we can draw the conclusion that the PCON not only remains integrated heptazine motif during the synthesis process, but also embed some new repeated N-C-O and N-C chains after a series of treatments. Furthermore, the intensity of C-O is decreased with an increase in temperature, indicating the interruption of chain has occurred. To further understand the interruption of PCON, TG analysis has been carried out. As shown in Fig. S7, the weight loss in the range 420–550  $^\circ\text{C}$  was contributed to the pyrolyzation of C-O-C. Therefore, appropriate calcination temperature will result in different amounts of C-N and N-C-O units. From the Table S4 and S5, the PCON-1 and PCON-3 occupied the maximum amount of N-C-O and C-N units, respectively. It is suggested that embed different linkers will cause built-in electric field to promote the separation of electrons and holes. As shown in Fig. S8, the specific surface area of PCON-2 is ( $19.0\text{ m}^2\text{ g}^{-1}$ ), which is larger than that of the  $\text{g-C}_3\text{N}_4$  ( $12.7\text{ m}^2\text{ g}^{-1}$ ),  $\text{C}_3\text{N}_5$  ( $18.3\text{ m}^2\text{ g}^{-1}$ ), PCON-1 ( $16.7\text{ m}^2\text{ g}^{-1}$ ), and PCON-3 ( $12.2\text{ m}^2\text{ g}^{-1}$ ), respectively. According to XPS, XRD, FI-IR and  $^{13}\text{C}$ NMR analysis, the C-N and N-C-O units are successfully introduced into the framework of poly(heptazine imide).

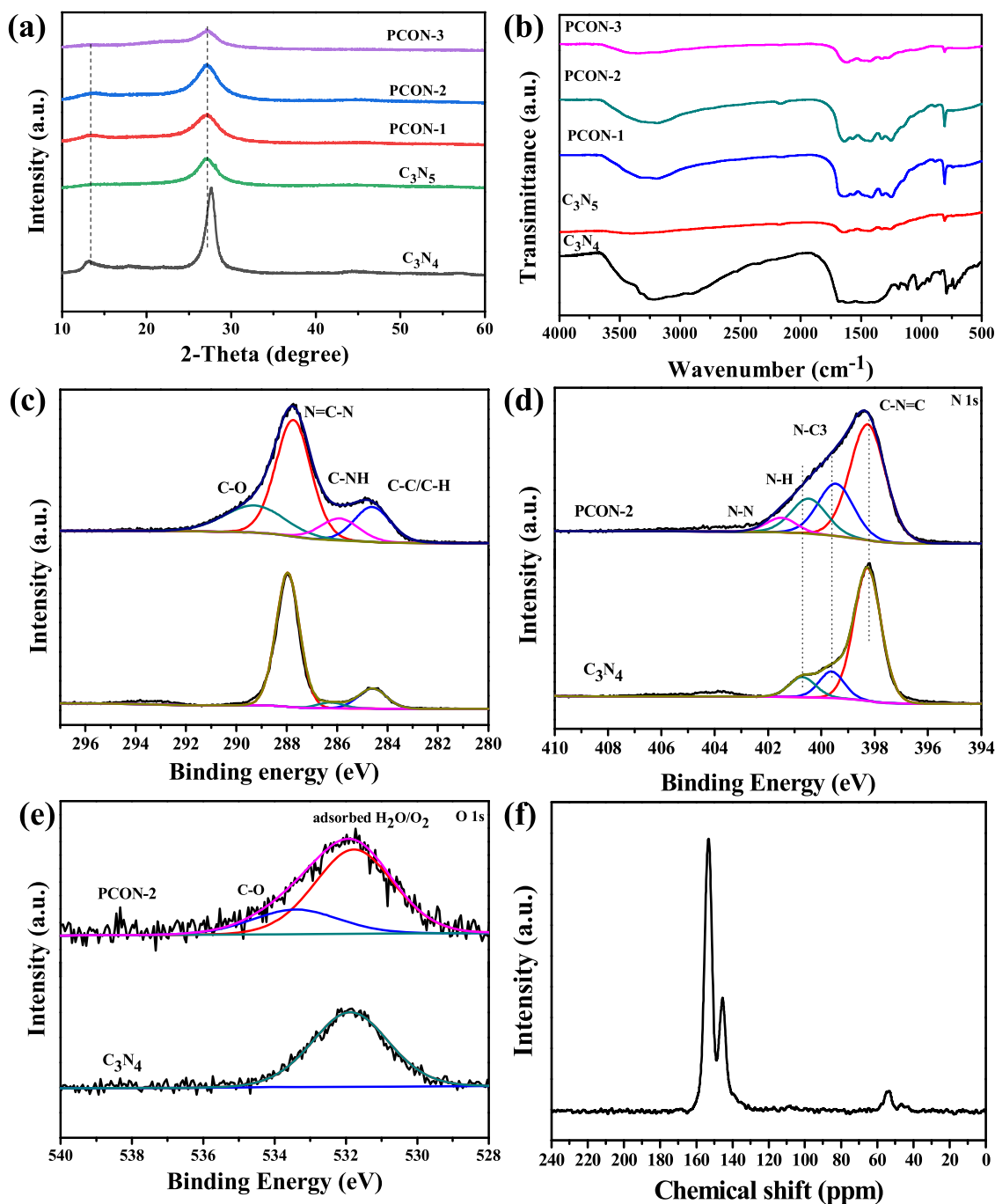


**Fig. 2.** (a) XRD patterns of as-fabricated sample, (b) FTIR spectra of as-fabricated samples, (c) High-resolution XPS spectra of PCON-2 (c) C 1 s, (d) N 1 s and (e) O 1 s, (f) Solid-state  $^{13}C$  NMR spectra of PCON-2.

### 3.2. Photocatalytic $NH_3$ conversion

In this experiment, the efficiency of photocatalytic nitrogen fixation was measured without any sacrificial agent and cocatalyst under the  $N_2$ -saturated water and visible light ( $\lambda > 420$  nm) radiation. The  $NH_3$  formation rates of all catalysts were measured by Nessler's reagent and calibration by the  $^1H$ NMR (Fig. S9 and S10, SI). As shown in Fig. 3a, the average  $NH_3$  production rate over g- $C_3N_4$ ,  $C_3N_5$ , PCON-1, PCON-2 and PCON-3 is ca. 3.7, 15.00, 39.41, 49.11 and 28.49  $\mu mol\ g^{-1}\ h^{-1}$ , respectively. The PCON-2 exhibits excellent  $NH_3$  production rate, which is 11 times higher than  $C_3N_4$ , and superior to the reported  $C_3N_4$  based composite (Table S6, SI). The kinetic experiment of nitrogen fixation was measured and found that the efficiency of nitrogen fixation also

increases with time (Fig. S11). The apparent quantum efficiency (AQE) of PCON-2 also has been investigated under different monochromatic light illumination [39]. As shown in Fig. 3b, the AQE could reach up to 1.25% at 450 nm. It is noted that the photocatalytic performance of nitrogen reduction over PCON-2 still remained a satisfactory activity even under 750 nm.

infrared light irradiation, indicating PCON-2 as an efficient photocatalyst for nitrogen reduction under visible and near-infrared illumination without any sacrificial agent and cocatalyst. At the same time, the quantum efficiency of  $C_3N_5$  was also tested. As shown in Fig. S12 (SI), the quantum efficiency of  $C_3N_5$  was much lower than PCON-2 at the same wavelength, indicating the unsymmetrical linker could significantly enhance the nitrogen fixation efficiency. To ensure the ammonia

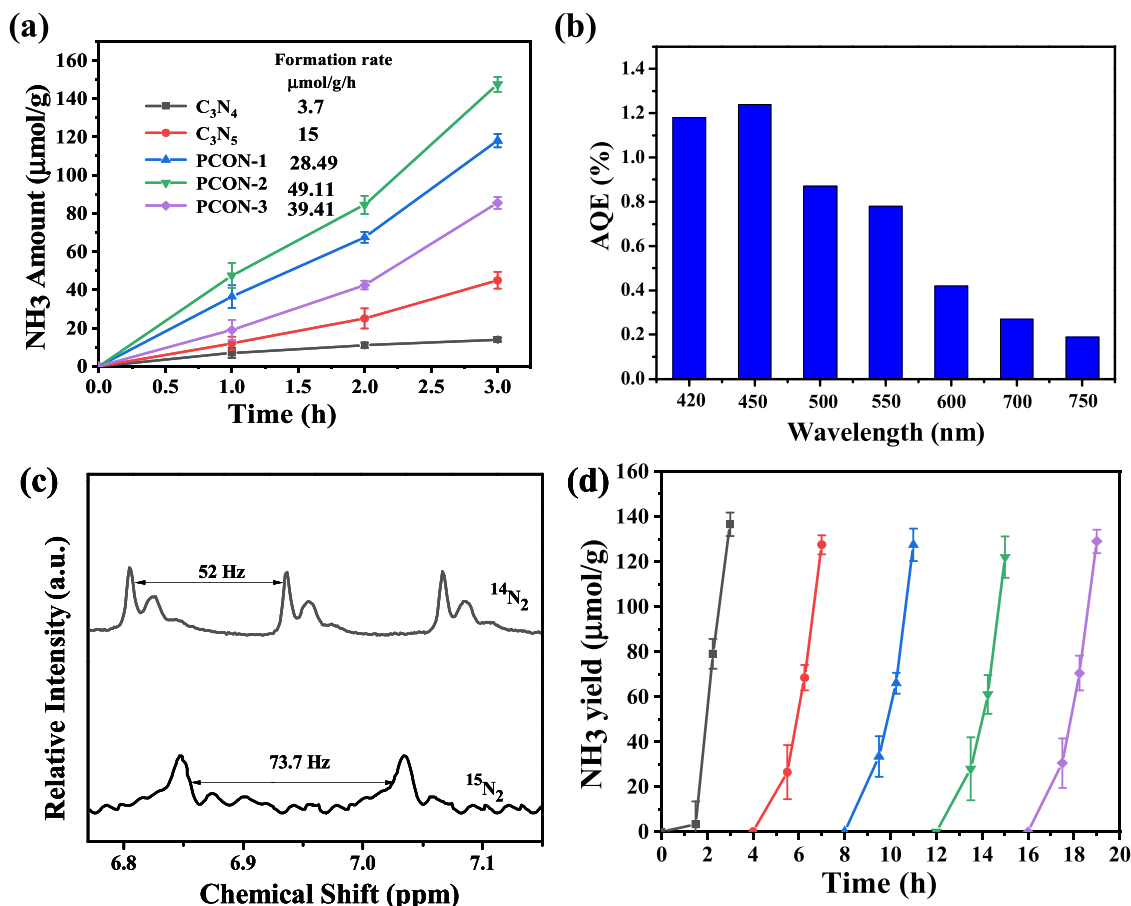


Fig. 3. (a) NH<sub>3</sub> evolution rates over as prepared catalysts, (b) apparent quantum efficiency (AQE), (c) <sup>1</sup>H NMR spectra of solution after photocatalytic N<sub>2</sub> fixation, and (d) cycling test over PCON-2.

derived from the photoreduction of N<sub>2</sub>, the blank experiments in Ar atmosphere were carried out. There is no detection of products when no catalysts or light is used. Further, the isotopically labeled <sup>15</sup>N<sub>2</sub> gas was also used to confirm the source of ammonia. As expected, the generation of <sup>14</sup>NH<sub>4</sub><sup>+</sup> and <sup>15</sup>NH<sub>4</sub><sup>+</sup> were determined from the <sup>1</sup>H NMR spectra after visible light irradiation for 3 h. It is unambiguously demonstrated that the ammonia detected in the current system was originated from N<sub>2</sub> photofixation, rather than some other nitrogen source. The stability of PCON was also examined. The nitrogen fixation rate of PCON-2 is no noticeable change after five consecutive cycles under visible light irradiation, indicating its high stability of structure, which can be further confirmed by the XRD and FT-IR spectra (Fig. S13, SI).

### 3.3. Mechanism of photocatalytic reaction

The energy band position is regarded as the thermodynamic factor in the PNRR. Therefore, the light absorption property of g-C<sub>3</sub>N<sub>4</sub>, C<sub>3</sub>N<sub>5</sub>, PCON-1, PCON-2 and PCON-3 were investigated via UV-vis/DRS. As shown in Fig. 4a, the absorption edge of PCON displays obviously shift to the infrared region, implying more charge carriers can be produced under the light illumination. There is a weak absorption band at 387 nm, which is attributed to  $\pi \rightarrow \pi^*$  transition in the conjugate network [40]. Besides, a broad absorption peak at approximately 459 nm is related to the  $n \rightarrow \pi^*$  transitions, which caused by the distortion of symmetric heptazine buckles. It is also suggested that a lone pairs on the edge of the long chains of the heptazine rings [41]. The lone pairs are the adsorption and activation of N<sub>2</sub>. On the one hand, the light response significantly extended into the near IR region. As shown in Fig. 4b, according to the UV-Vis spectrum, the band gap width of g-C<sub>3</sub>N<sub>4</sub>, C<sub>3</sub>N<sub>5</sub>, PCON-1, PCON-2

and PCON-3 are 2.85, 2.63, 2.41, 2.12, 2.25 eV, respectively. Fig. S14a exhibits the positive slope of the linear plots of all catalysts, which implies the n-type characteristics of all catalysts [39]. The calculated conduction band edges of g-C<sub>3</sub>N<sub>4</sub>, C<sub>3</sub>N<sub>5</sub>, PCON-1, PCON-2 and PCON-3 are -1.13, -0.9, -0.78, -0.82 and -0.81 eV, respectively. Thus, the valence band alignments could be obtained and shown in Fig. S14b. This result shows the narrowed band gap not only helps to improve the production of the charge carriers but also conducive to overcome the thermodynamic obstruction of photocatalytic nitrogen fixation in pure water.

For comprehensive mechanism insights of the enhanced photocatalytic performance, the separation efficiency of photoexcited carriers was tested by PL spectra and photocurrent. As shown in Fig. 4d, steady-state PL ( $\lambda_{\text{ex}}=380$  nm) shows, the recombination of photogenerated carriers is substantially suppressed by the incorporation of different linkers. In addition, the peaks of PCON are shifts to longer wavelengths. It can account for the  $n \rightarrow \pi^*$  transition in the PCON, suggesting the accelerated transfer of the photoexcited electrons and further inhibited their recombination with holes. As shown in Fig. 4e and Table S7, steady-state time-resolved photoluminescence (PL) spectroscopy is also used to measure the excitonic processes. The fitted fluorescence lifetime of C<sub>3</sub>N<sub>4</sub> and PCON-2 could reach 7.11 and 7.79 ns, respectively, indicating the enhanced separation and transfer of charge carriers in the poly(heptazine imide) framework. To understand the charge carrier transferability of as prepared samples, the photocurrent and EIS measurement have been carried out. As depicted in Fig. 4f, the photocurrent intensities of catalysts are in the order of PCON-2 > PCON-1 > PCON-3 > C<sub>3</sub>N<sub>5</sub> > C<sub>3</sub>N<sub>4</sub>. From the EIS (Fig. 4g) results, the radius of PCON-2 is smaller than that of other catalysts, indicating that it is more capable of

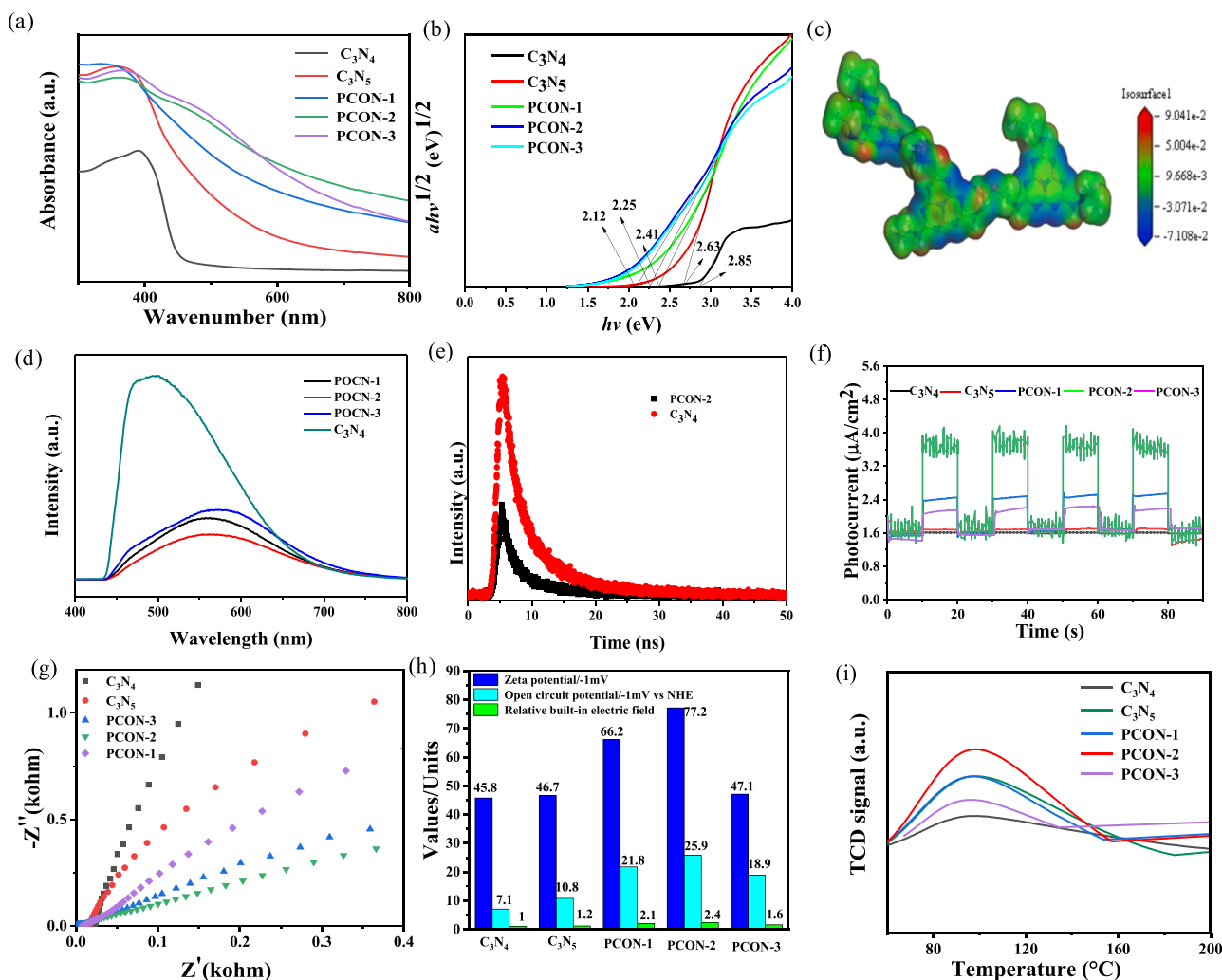


**Fig. 4.** (a) UV–vis absorption, (b) the corresponding Tauc plots, (c) electrostatic potential of PCON-2, (d) Steady-state PL spectra, (e) time-resolved PL spectra, (f) photocurrent responses, (g) electrochemical impedance spectroscopy of photocatalyst, (h) characterization of built-in electric field over as prepared samples and (i)  $N_2$ -TPD spectra of fabricated samples.

charge transfer efficiency. These results are consistent with the PL results. Electrochemical and fluorescence tests show that the addition of C–N and C–O–C chains inhibits the recombination of electrons and holes to a certain extent, and accelerates the transport of carriers, thereby improving the photocatalytic performance. Interestingly, the PCON-1 and PCON-3 occupied the maximum amount of N–C–O and C–N units, respectively. While the carrier transfer capacity is lower than the PCON-2, indicating different linker will cause built-in electric field to promote the separation of electrons and holes. The built-in electric field is composed of two crucial influence factors containing the surface charge density and surface voltage, which can be represented by zeta potential and open circuit potential of the photocatalysts [42,43]. As shown in Fig. 4h, the open circuit potential and the zeta potential of PCON-2 is 25.9 and  $-77.2$  mV, respectively. If the built-in electric field of  $C_3N_4$  is deemed to 1.0, then the relative quantitative values for  $C_3N_5$ , PCON-1, PCON-2 and PCON-3 are 1.2, 2.1, 2.4 and 1.6. It is implied that the introduction of different linker could further improve the separation of charge via the built-in electric field.

To get insight into the transfer behavior of electrons and holes, DFT calculation was performed. As shown in Fig. S15 (SI), the VB of PCON mainly contributed to hybridized N 2p, N 1 s, C 2p and O 2p orbitals, while the  $C_3N_4$  is derived from N 2p, N 1 s and C 2p orbitals (Fig. S16, SI) [44]. In addition, the N–C–O and N–C linker in PCON are conducive to the HOMO (Fig. S17, SI), the LUMO orbital of PCON is mainly consisted of

heptazine unit and N–C linker. However, the HOMO and LUMO orbital of  $C_3N_4$  mainly consisted of heptazine unit (Fig. S18, SI). It means that the transport of the photogenerated electrons from one heptazine unit to another one through the linker is enhanced, resulting in the hinder of symmetric heptazine units of charge has been cleared. To further disclose the source of the built-in electric field, we use the differential charges density to investigate the charges distribution of the PCON (Fig. 4c and S19, SI). The N–C–O bridges possessed more electrons gather than N–C linker, indicating linker can be act as reactive site and build in the electric field to further facilitate electron transfer in heptazine units. As shown in Fig. S20, the Mulliken charge of PCON further shown that the inserted electronic bridge could be the source of building in the electric field for facilitating electron transfer in heptazine units.

In order to study the surface properties of PCON, the  $N_2$ -TPD have been carried out. As shown in Fig. 4i, the embedding chains in PCON could significantly improve the adsorption capacity of  $N_2$ , which was conducive to nitrogen fixation in pure water. To obtain detail information about the surface properties over PCON, DFT calculations were also performed to obtain the atomic-level optimized coordination geometry of  $N_2$  on the surface of PCON (Fig. S21, SI). It is obviously observed that  $N_2$  molecule was preferred to adsorbed in the surface of the embedded N linker. Besides, the  $N\equiv N$  bond on the embedded N linker was increased to  $1.104 \text{ \AA}$ , indicating the inserted linker in the PCON-2 reasonably conducive to the activation of  $N_2$  molecules. The hydrophilia is an

important role in the surface properties. As shown in Fig. S22 (SI), the contact angle of PCON is in the order PCON-1 < PCON-2 < PCON-3 < C<sub>3</sub>N<sub>5</sub> < C<sub>3</sub>N<sub>4</sub>, indicating the introduced polar functional groups in the terminal of PCON contribute to hydrophilia. Because of the influence of adjacent CH<sub>2</sub> group, the hydrophobic effect has occurred in PCON the by the embed different amount of linker. It is suggested that a suppression effect on photocatalytic hydrogen production over PCON with different CH<sub>2</sub> group. To further unravel the behavior of N<sub>2</sub> on the PCON-2, in situ infrared spectroscopic measurement was also investigated. As depicted in Fig. S23a, two small peaks appear at 3360 and 1624 cm<sup>-1</sup> belong to adsorbed H<sub>2</sub>O and N<sub>2</sub>, respectively [45]. The sharp peaks at 3555, 2874 and 1577 cm<sup>-1</sup> are contributed to  $\nu(\text{N}-\text{H})$ ,  $\text{NH}_4^+$  and  $\text{NH}_3$  stretching vibration, indicating a large amount of  $\text{NH}_3$  was produced from the photocatalytic N<sub>2</sub> fixation [45]. A broad band at 2103 cm<sup>-1</sup> is assigned to N=N stretching vibration, suggesting the N<sub>2</sub> confront the reduction of  $\text{N}\equiv\text{N}$  to  $\text{N}=\text{N}$  pathway. Importantly, a small band formed at 2333 cm<sup>-1</sup> is assigned to N<sub>2</sub> chemisorbed on the Brønsted acid site, demonstrating the N<sub>2</sub> adsorbed on the surface of N-N linker [46]. In addition, the peak of N-C-O and N-C have appeared in the N<sub>2</sub> and H<sub>2</sub>O environment, whereas almost disappeared in the H<sub>2</sub>O environment (Fig. S23b, SI). Moreover, the peak of heptazine emerged in the H<sub>2</sub>O environment, suggesting the N linker prior participate in the activation of nitrogen to H<sup>+</sup>. Therefore, a suppression effect of photocatalytic hydrogen will occurred in the PCON. In a word, the embed linker and heptazine units were chosen as the active site for the N<sub>2</sub> and OH<sup>-</sup>, respectively, which were contribute to enhance the nitrogen fixation efficiency.

Based on the above results and reported works [47,48], a plausible mechanism for the N<sub>2</sub> photofixation over PCON is proposed in Fig. 5. Under light irradiation, the heptazine units in PCON-2 were excited and produced electron and hole pairs. Due to the embed electronic channel, the photogenerated electrons will transfer to embedded linker for enhancing the carriers separation efficiency. Meanwhile, the adsorbed N<sub>2</sub> on the linker site will reaction with the electrons, followed by participating in H<sup>+</sup> to produce NH<sub>3</sub>. On the other hand, the holes generated in the heptazine unit will react with water to produce O<sub>2</sub>.

#### 4. Conclusion

In conclusion, we successfully embedded C-N and N-C-O units in the poly(heptazine imide) photocatalyst via a simple monomer-directed copolymerization strategy. Impressively, PCON exhibited remarkable activity in N<sub>2</sub> photofixation in the pure water under visible light irradiation, attaining an NH<sub>3</sub> production rate of 49.11  $\mu\text{mol g}^{-1} \text{h}^{-1}$  without any cocatalyst at room temperature, which was 11 times clearly higher than g-C<sub>3</sub>N<sub>4</sub> and the other reported metal-free catalyst. More importantly, the PCON still maintain considerable NH<sub>3</sub> production under the near-IR (750 nm) monochromatic light illumination. Further mechanistic studies demonstrated that the embedded C-N and N-C-O units in the poly(heptazine imide) photocatalyst induced  $n-\pi^*$  transitions for enabling the photocatalyst extend to the near-IR light response. In addition, DFT calculation revealed the different linker provide a carriers channel to improve the separation of photocarriers. And last but not least, the inserted linker in the PCON reasonably contribute to the activation and adsorption of N<sub>2</sub> molecules. It is expected that the linker engineering could open up new concept and opportunities in boosting photocatalytic N<sub>2</sub> fixation reactions.

#### CRedit authorship contribution statement

**Shilian Yang:** Methodology, Investigation, Data curation. **Xiaoxu Deng:** Conceptualization, Software. **Peng Chen:** Conceptualization, Supervision, Writing – review & editing, Funding acquisition. **Tianxiang Zhao:** Supervision, Investigation. **Fei Liu:** Investigation, Funding acquisition. **Chaoyong Deng:** Supervision, Formal analysis. **Shuang-Feng Yin:** Supervision, Investigation.

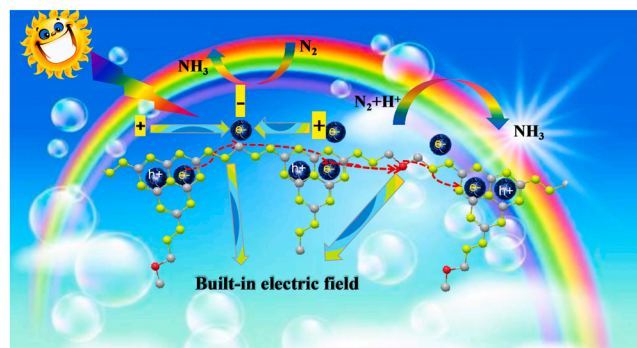


Fig. 5. Plausible mechanism for the photocatalytic N<sub>2</sub> fixation over PCON-2 under visible light irradiation.

#### Declaration of Competing Interest

The authors declare that they have no known competing financial interests or personal relationships that could have appeared to influence the work reported in this paper.

#### Acknowledgements

This project was financially supported by Young Science and Technology Talents Development Project of Education Department in Guizhou Province (No. 2022144), Guizhou Provincial Science and Technology Foundation (No. 2021069), and the National Natural Science Foundation of China (No. 21725602, 21975069). The authors would like to thank Shiyanjia Lab ([www.shiyanjia.com](http://www.shiyanjia.com)) for materials characterizations.

#### Appendix A. Supporting information

Supplementary data associated with this article can be found in the online version at [doi:10.1016/j.apcatb.2022.121370](https://doi.org/10.1016/j.apcatb.2022.121370).

#### References

- [1] C. Ling, Y. Zhang, Q. Li, X. Bai, L. Shi, J. Wang, New mechanism for N<sub>2</sub> reduction: The essential role of surface hydrogenation, *J. Am. Chem. Soc.* 141 (2019) 18264–18270.
- [2] M. Philippi, K. Kitzinger, J.S. Berg, B. Tschitschko, A.T. Kidane, S. Littmann, H. K. Marchant, N. Storelli, L.H.E. Winkel, C.J. Schubert, W. Mohr, M.M.M. Kuypers, Purple sulfur bacteria fix N<sub>2</sub> via molybdenum-nitrogenase in a low molybdenum proteozone ocean analogue, *Nat. Commun.* 12 (2021) 4774.
- [3] C. Lv, C. Yan, G. Chen, Y. Ding, J. Sun, Y. Zhou, G. Yu, An Amorphous noble-metal-free electrocatalyst that enables nitrogen fixation under ambient conditions, *Angew. Chem. Int. Ed.* 57 (2018) 6073–6076.
- [4] G. Chen, S. Ren, L. Zhang, H. Cheng, Y. Luo, K. Zhu, L.-X. Ding, H. Wang, Advances in electrocatalytic N<sub>2</sub> reduction-strategies to tackle the selectivity challenge, *Small Methods* 13 (2019), 1800337.
- [5] J. Lee, X. Liu, A. Kumar, Y. Hwang, E. Lee, J. Yu, Y.D. Kim, H. Lee, Rational catalyst design for N<sub>2</sub> reduction under ambient conditions: strategies toward enhanced conversion efficiency, *Chem. Sci.* 12 (2021) 9619–9629.
- [6] Z. Zhao, D. Wang, R. Gao, G. Wen, M. Feng, G. Song, J. Zhu, D. Luo, H. Tan, X. Ge, W. Zhang, Y. Zhang, L. Zheng, H. Li, Z. Chen, Magnetic-field-stimulated efficient photocatalytic N<sub>2</sub> fixation over defective BaTiO<sub>3</sub> perovskites, *Angew. Chem. Int. Ed.* 60 (2021) 11910–11918.
- [7] W. Wang, H. Zhang, S. Zhang, Y. Liu, G. Wang, C. Sun, H. Zhao, Potassium-ion-assisted regeneration of active cyano groups in carbon nitride nanoribbons: Visible-light-driven photocatalytic nitrogen reduction, *Angew. Chem. Int. Ed.* 58 (2019) 16644–16650.
- [8] L. Shi, Y. Yin, S. Wang, H. Sun, Rational catalyst design for N<sub>2</sub> reduction under ambient conditions: strategies toward enhanced conversion efficiency, *ACS Catal.* 10 (2020) 6870–6899.
- [9] C. Guo, J. Ran, A. Vasileff, S. Qiao, Rational design of electrocatalysts and photo (electro)catalysts for nitrogen reduction to ammonia (NH<sub>3</sub>) under ambient conditions, *Energy Environ. Sci.* 11 (2018) 45–56.
- [10] Y. Zhao, R. Shi, X. Bian, C. Zhou, Y. Zhao, S. Zhang, F. Wu, G.I.N. Waterhouse, L. Wu, C. Tung, T. Zhang, Ammonia detection methods in photocatalytic and electrocatalytic experiments: How to Improve the reliability of NH<sub>3</sub> production rates? *Adv. Sci.* 6 (2019), 1802109.

- [11] Z. Wang, X. Hu, Z. Liu, G. Zou, G. Wang, K. Zhang, Recent developments in polymeric carbon Nitride-Derived photocatalysts and electrocatalysts for nitrogen fixation, *ACS Catal.* 9 (2019) 10260–10278.
- [12] W. Wang, H. Zhang, S. Zhang, Y. Liu, G. Wang, C. Sun, H. Zhao, Potassium-ion-assisted regeneration of active cyano groups in carbon nitride nanoribbons: Visible-light-driven photocatalytic nitrogen reduction, *Angew. Chem. Int. Ed.* 58 (2019) 16644–16650.
- [13] M.Y. Ye, S. Li, X. Zhao, N.V. Tarakina, C. Teutloff, W.Y. Chow, R. Bittl, A. Thomas, Cobalt-exchanged poly(heptazine imides) as transition Metal-N<sub>x</sub> electrocatalysts for the oxygen evolution reaction, *Adv. Mater.* 32 (2020), 1903942.
- [14] H. Schlöberger, J. Kroger, G. Savasci, M.W. Terban, S. Bette, I. Moudrakovski, V. Duppel, F. Podjaski, R. Siegel, J. Senker, R.E. Dinnebier, C. Ochsenfeld, B. V. Lotsch, Structural insights into poly(heptazine imides): a light-storing carbon nitride material for dark photocatalysis, *Chem. Mater.* 31 (2019) 7478–7486.
- [15] S. Mazzanti, S. Cao, K.T. Brummelhuis, A. Völkel, J. Khamrai, D.I. Sharapa, S. Youk, T. Heil, N.V. Tarakina, V. Strauss, I. Ghosh, B. König, M. Oschatz, M. Antonietti, A. Savateev, All-organic Z-scheme photoreduction of CO<sub>2</sub> with water as the donor of electrons and protons, *Appl. Catal. B* 285 (2021), 119773.
- [16] Y. Wang, S.Z.F. Phua, G. Dong, X. Liu, B. He, Q. Zhai, Y. Li, C. Zheng, H. Qian, Z. Li, Y. Zhao, Structure tuning of polymeric carbon nitride for solar energy conversion: From nano to molecular scale, *Chem* 5 (2019) 2775–2813.
- [17] V.W.-h. Lau, V.W.-z. Yu, F. Ehrat, T. Botari, I. Moudrakovski, T. Simon, V. Duppel, E. Medina, J.K. Stolarczyk, J. Feldmann, V. Blum, B.V. Lotsch, Urea-modified carbon nitrides: Enhancing photocatalytic hydrogen evolution by rational defect engineering, *Adv. Energy Mater.* 7 (2017), 1602251.
- [18] C. Huang, Y. Wen, J. Ma, D. Dong, Y. Shen, S. Liu, H. Ma, Y. Zhang, Unraveling fundamental active units in carbon nitride for photocatalytic oxidation reactions, *Nat. Commun.* 12 (2021) 320.
- [19] V.W. Lau, I. Moudrakovski, T. Botari, S. Weinberger, M.B. Mesch, V. Duppel, J. Senker, V. Blum, B.V. Lotsch, Rational design of carbon nitride photocatalysts by identification of cyanamide defects as catalytically relevant sites, *Nat. Commun.* 7 (2016) 12165.
- [20] P. Kumar, E. Vahidzadeh, U.K. Thakur, P. Kar, K.M. Alam, A. Goswami, N. Mahdi, K. Cui, G.M. Bernard, V.K. Michaelis, K. Shankar, C<sub>3</sub>N<sub>4</sub>: a low bandgap semiconductor containing an azo-linked carbon nitride framework for photocatalytic, photovoltaic and adsorbent applications, *J. Am. Chem. Soc.* 141 (2019) 5415–5436.
- [21] G. Jia, Y. Wang, X. Cui, Z. Yang, L. Liu, H. Zhang, Q. Wu, L. Zheng, W. Zheng, Asymmetric embedded benzene ring enhances charge transfer of carbon nitride for photocatalytic hydrogen generation, *Appl. Catal. B* 258 (2019), 117959.
- [22] X.-W. Guo, S.-M. Chen, H.-J. Wang, Z.-M. Zhang, H. Lin, L. Song, T.-B. Lu, Single-atom molybdenum immobilized on photoactive carbon nitride as efficient photocatalysts for ambient nitrogen fixation in pure water, *J. Mater. Chem. A* 7 (2019) 19831–19837.
- [23] L. Kang, B. Wang, J. Zeng, Z. Cheng, J. Li, J. Xu, W. Gao, K.F. Chen, Degradable dual superlyophobic lignocellulosic fibers for high-efficiency oil/water separation, *Green. Chem.* 22 (2020) 504–512.
- [24] R. Saleem, A. Adnan, M. Hanif, M. Saleem, K.-H. Lee, F.A. Qureshi, Synthesis and application of sulfonated adipic dihydrazide formaldehyde-based resins under different molar ratios as effective leather retanning agents, *Iran. Polym. J.* 23 (2013) 69–78.
- [25] Y. Yu, S. Wu, J. Gu, R. Liu, Z. Wang, H. Chen, F. Jiang, Visible-light photocatalytic degradation of bisphenol A using cobalt-to-oxygen doped graphitic carbon nitride with nitrogen vacancies via metal-to-ligand charge transfer, *J. Hazard. Mater.* 384 (2020), 121247.
- [26] H. Ou, X. Chen, L. Lin, Y. Fang, X. Wang, Biomimetic donor-acceptor motifs in conjugated polymers for promoting exciton splitting and charge separation, *Angew. Chem. Int. Ed.* (2018) 8729–8733.
- [27] H.-B. Fang, X.-H. Zhang, J. Wu, N. Li, Y.-Z. Zheng, X. Tao, Fragmented phosphorus-doped graphitic carbon nitride nanoflakes with broad sub-bandgap absorption for highly efficient visible-light photocatalytic hydrogen evolution, *Appl. Catal. B* 225 (2018) 397–405.
- [28] M. Wu, J. Zhang, B.-B. He, H.-W. Wang, R. Wang, Y.-S. Gong, In-situ construction of coral-like porous P-doped g-C<sub>3</sub>N<sub>4</sub> tubes with hybrid 1D/2D architecture and high efficient photocatalytic hydrogen evolution, *Appl. Catal. B* 241 (2019) 159.
- [29] X. Song, X. Li, X. Zhang, Y. Wu, C. Ma, P. Huo, Y. Yan, Fabricating C and O co-doped carbon nitride with intramolecular donor-acceptor systems for efficient photoreduction of CO<sub>2</sub> to CO, *Appl. Catal. B* 268 (2020), 118736.
- [30] Q. Han, Z. Cheng, J. Gao, Y. Zhao, Z. Zhang, L. Dai, Q. Qu, Mesh-on-mesh graphitic-C<sub>3</sub>N<sub>4</sub>@graphene for highly efficient hydrogen evolution, *Adv. Funct. Mater.* 27 (2017), 1606352.
- [31] J. Yuan, X. Yi, Y. Tang, C. Liu, S. Luo, Efficient photocatalytic hydrogen evolution and CO<sub>2</sub> reduction: Enhanced light absorption, charge separation, and hydrophilicity by tailoring terminal and linker units in g-C<sub>3</sub>N<sub>4</sub>, *ACS Appl. Mater. Interfaces* 12 (2020) 19607–19615.
- [32] L. Ming, H. Yue, L. Xu, F. Chen, Hydrothermal synthesis of oxidized g-C<sub>3</sub>N<sub>4</sub> and its regulation of photocatalytic activity, *J. Mater. Chem. A* 2 (2014) 19145–19149.
- [33] J. Wu, N. Li, X.-H. Zhang, H.-B. Fang, Y.-Z. Zheng, X. Tao, Heteroatoms binary-doped hierarchical porous g-C<sub>3</sub>N<sub>4</sub> nanobelts for remarkably enhanced visible-light-driven hydrogen evolution, *Appl. Catal. B* 226 (2018) 61–70.
- [34] S. Guo, Z.P. Deng, M. Li, B. Jiang, C. Tian, Q. Pan, H. Fu, Phosphorus-doped carbon nitride tubes with a layered micro-nanostructure for enhanced visible-light photocatalytic hydrogen evolution, *Angew. Chem. Int. Ed.* 55 (2016) 1830–1834.
- [35] J. Zhang, B. Xin, C. Shan, W. Zhang, D. Dionysiou, B. Pan, Roles of oxygen-containing functional groups of O-doped g-C<sub>3</sub>N<sub>4</sub> in catalytic ozonation: Quantitative relationship and first-principles investigation, *Appl. Catal. B* 292 (2021), 120155.
- [36] Y. Li, X. Xu, J. Wang, W. Luo, Z. Zhang, X. Cheng, J. Wu, Y. Yang, G. Chen, S. Sun, L. Wang, Post-redox engineering electron configurations of atomic thick C<sub>3</sub>N<sub>4</sub> nanosheets for enhanced photocatalytic hydrogen evolution, *Appl. Catal. B* 270 (2020), 118855.
- [37] Z. Li, C. Chen, Q. Yang, Q. Liu, Z. Zhang, X. Fang, Modifying the bridging N atoms of polymeric carbon nitride to achieve highly enhanced photocatalytic hydrogen evolution, *Appl. Surf. Sci.* 530 (2020), 147287.
- [38] J. Kröger, A. Jiménez-Solano, G. Savasci, P. Rovó, I. Moudrakovski, K. Küster, H. Schlöberger, H.A. Vignolo-González, V. Duppel, L. Grunenberg, C.B. Dayan, M. Sitti, F. Podjaski, C. Ochsenfeld, B.V. Lotsch, Interfacial engineering for improved photocatalysis in a charge storing 2D carbon nitride: Melamine functionalized poly(heptazine imide), *Adv. Energy Mater.* 11 (2020), 2003016.
- [39] S. Yang, Q. Wang, Q. Wang, G. Li, T. Zhao, P. Chen, F. Liu, S.-F. Yin, Linkage engineering mediated carriers transfer and surface reaction over carbon nitride for enhanced photocatalytic activity, *J. Mater. Chem. A* 9 (2021) 21732–21740.
- [40] J.-Y. Tang, X. Kong, B.-J. Ng, Y.-H. Chew, A.R. Mohamed, S.-P. Chai, Midgap-state-mediated two-step photoexcitation in nitrogen defect-modified g-C<sub>3</sub>N<sub>4</sub> atomic layers for superior photocatalytic CO<sub>2</sub> reduction, *Catal. Sci. Technol.* 9 (2019) 2335–2343.
- [41] Y. Chen, B. Wang, S. Lin, Y. Zhang, X. Wang, Activation of n→π\* transitions in two-dimensional conjugated polymers for visible light photocatalysis, *J. Phys. Chem. C* 118 (2014) 29981–29989.
- [42] H. Zhang, X. Chen, Z. Zhang, K. Yu, W. Zhu, Y. Zhu, Highly-crystalline triazine-PDI polymer with an enhanced built-in electric field for full-spectrum photocatalytic phenol mineralization, *Appl. Catal. B* 287 (2021), 119957.
- [43] Z. Zhang, X. Chen, H. Zhang, W. Liu, W. Zhu, Y. Zhu, A highly crystalline perylene imide polymer with the robust built-in electric field for efficient photocatalytic water oxidation, *Adv. Mater.* 32 (2020), 1907746.
- [44] X. Zhou, C. Zhao, B. Li, J. Chen, L. Wang, DFT study of interaction between HCHO molecule and tri-s-triazine g-C<sub>3</sub>N<sub>4</sub> surface, *Mol. Catal.* 483 (2020), 110718.
- [45] P. Li, Z. Zhou, Q. Wang, M. Guo, S. Chen, J.X. Low, R. Long, W. Liu, P. Ding, Y. Wu, Y. Xiong, Visible-light-driven nitrogen fixation catalyzed by Bi<sub>5</sub>O<sub>7</sub>Br nanostructures: Enhanced performance by oxygen vacancies, *J. Am. Chem. Soc.* 142 (2020) 12430–12439.
- [46] Y. Shiraiishi, M. Hashimoto, K. Chishiro, K. Moriyama, S. Tanaka, T. Hirai, Photocatalytic dinitrogen fixation with water on bismuth oxychloride in chloride solutions for solar-to-chemical energy conversion, *J. Am. Chem. Soc.* 142 (2020) 7574–7583.
- [47] J. Yang, H. Bai, Y. Guo, H. Zhang, R. Jiang, B. Yang, J. Wang, J.C. Yu, Photodriven disproportionation of nitrogen and its change to reductive nitrogen photofixation, *Angew. Chem. Int. Ed.* 6 (2021) 927–936.
- [48] X.-W. Guo, S.-M. Chen, H.-J. Wang, Z.-M. Zhang, H. Lin, L. Song, T.-B. Lu, Single-atom molybdenum immobilized on photoactive carbon nitride as efficient photocatalysts for ambient nitrogen fixation in pure water, *J. Mater. Chem. A* 7 (2019) 19831–19837.